Healing Surface Defects with Nanoparticle-Filled Polymer Coatings: Effect of Particle Geometry

Kurt A. Smith, Sandeep Tyagi, and Anna C. Balazs*

Department of Chemical and Petroleum Engineering, University of Pittsburgh, Pittsburgh, Pennsylvania 15261

Received July 12, 2005; Revised Manuscript Received September 26, 2005

ABSTRACT: Using computational models, we investigate how the aspect ratio of nanoparticle fillers within a polymer coating affects the ability of the film to heal nanoscale defects in the underlying substrate. We first consider the interactions between the filled polymer melt and a flat surface and show that the depletion attraction between the nanoparticles and this substrate depends strongly on this aspect ratio. In particular, the rodlike particles experience a significantly stronger attraction to the substrate than spherical fillers. We quantify these interactions by measuring the effective potential between a particle and surface as well as between two particles in the melt. We then consider the case of a surface that contains a nanoscopic notch, which represents the damaged region. We show how tailoring the particles' aspect ratio provides a means of optimizing the localization of the particles into the notch. Morphologies obtained from molecular dynamics simulations are then used as input to a lattice spring model, which allows us to determine the mechanical properties of the coated surfaces. The results show that coatings filled with rodlike particles significantly reduce the stress concentrations at the notch. The application of such nanocomposite coatings could potentially yield defect-free surfaces that exhibit enhanced mechanical properties.

I. Introduction

One of the current challenges in designing "smart" materials is to create coatings that effectively heal defects in the underlying surface. Such coatings would significantly extend the lifetime and utility of manufactured components. Because of the push to fabricate nanoscale devices, there is a particular need to create materials for healing the nanoscale defects that arise in these devices. Whether localized in such miniature devices or more macroscopic components, nanoscale notches and scratches can have a substantially deleterious effect on the mechanical properties of the entire system. For example, the significant stress concentrations that occur at the tip of the notches[1,2] can ultimately lead to the propagation of cracks through the material and the degradation of mechanical behavior. Such nanoscopic defects are, however, difficult to detect,[3] making their repair especially difficult. What is needed is a "responsive" coating that can be readily applied to the system, such that when a defect appears, the coating effectively senses its presence and then causes the repair of the damaged area.

In recent studies,[1,2] we used computational modeling to examine how a molten polymer coating that contains spherical nanoparticles could be utilized to repair these nanoscale defects. In particular, we focused on a substrate that contained a nanoscopic notch and found that the particles within the polymer melt were driven to the surface by a polymer-induced, entropic "depletion attraction" (similar to that described in refs 4 and 5). The geometry of the system is shown in Figure 1. As illustrated in Figure 2, the particle and a wall each have an excluded volume that the monomer centers cannot enter. The excluded volume of a particle is equal to the particle volume plus a "depletion zone", a shell whose width is equal to the monomer radius. When the particle and wall are in contact, there is an overlap of their depletion zones, hence an increase in the enropy of the system due to the greater free volume available to the monomers. (A similar attraction exists between two particles.)

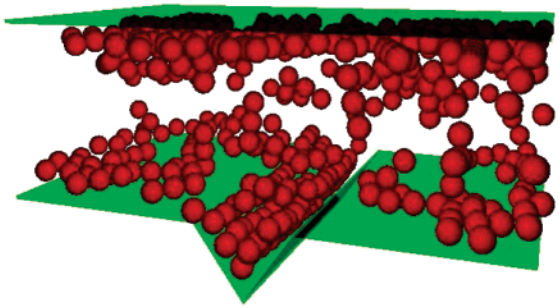

Figure 1. Geometry of the system used in the molecular dynamics simulations. Filler particles are shown in red, and the confining walls are shown in green. For clarity, the polymer chains are not shown. The lower wall contains a notch.

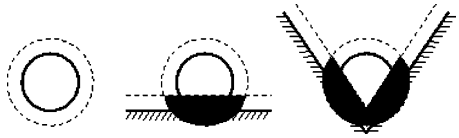

Figure 2. Each particle is surrounded by a "depletion zone" that monomer centers cannot enter, as indicated by the dashed line in the left image. A depletion zone also exists at a wall. In the middle figure, where a particle lies at a wall, the total volume available to the monomers is increased by the shaded overlap region of the two depletion zones. In the right figure, the particle is at a notch, and the total overlap region is greater, since the particle interacts with each side wall. The size of the overlap region depends on the notch angle. For small angles, where the side walls are nearly parallel, it is nearly double the size of the overlap region between a particle and a flat wall.

* E-mail: balazs1@engr.pitt.edu (A.C.B.) and ksmith@dorothy.che.pitt.edu (K.A.S.).

10.1021/ma0515127 CCC: $30.25
Published on Web 11/04/2005

This depletion attraction is even stronger within the notch (near the tip), where particles experience an attraction from both of the side walls[5] (see Figure 1). In other words, the polymers can further increase the volume available to them by sequestering particles into defects within the surface.[1,2] Thus, when new cracks or notches appear, the polymers will again induce a depletion attraction between the particles and the defect, since further localization of particles within the defects frees up new space within the film. In this manner, the particle-filled coating "senses" new damage and affects the desired repair.

This particle-filled coating can be applied as a finishing step in the processing of the component; upon cooling the coating would form a solid nanocomposite layer. In previous studies,[1,2] we assumed that this quench could occur sufficiently quickly that the positions of the polymers and particles were not perturbed by the rapid cooling. We then simulated the response of this solid system to an applied deformation and found that the particles localized in the notch significantly reduced the stress and strain concentrations and thereby effectively healed the damaged material.

In this study, we examine how the aspect ratio of the nanoparticles within the polymer melt affects both the localization of these fillers into the notch and the extent to which the mechanical properties of the damaged surface are restored. In particular, we fix the volume of the particle and simply vary its shape. This investigation is motivated by the hypothesis that the particle geometry should play an important role in the ability of the coating to repair the surface. We see two factors suggesting that a nonspherical shape might be optimal. The first is that the strength of the depletion attraction is related to the size of the spherical particle; a sphere of the same size as a monomer experiences no attraction to the surface while the strength of the attraction increases monotonically with sphere size.[1] Thus, larger spheres must be used in order to obtain a significant depletion attraction (see ref 1 and references therein). The drawback to this is that the bigger particles are not able to pack as closely into the narrow tip of the notch. In contrast, a high aspect ratio rod can be appropriately small in the radial dimension, yet potentially still feel a strong depletion attraction. This suggests the ability to drive particles very close to the notch tip. The second consideration is the effect of particle shape on packing. The higher the volume fraction of particles in a notch, the more fully it is healed.[1] While the optimal packing fraction for spheres is 0.74 (assuming a fcc or hcp structure), that of aligned rods (based on the close packing of circles in two dimensions) is 0.91. A recent study[6] has also shown that even for randomly packed objects, spheres do not achieve the highest possible packing fraction.

To test the above conjecture on the effect of particle shape, we first use molecular dynamics (MD) simulations to determine the distribution of the various particles. Once we obtain the equilibrium structure of the mixture from the MD simulations, we then use this information as the input into a micromechanics simulation in order to evaluate how the fillers modify the mechanical behavior of the system. As noted above, we assume that the filled melt is rapidly cooled to form the solid coating and that the morphology does not change under the rapid quench. Consequently, the location of the particles and polymers in the MD lattice is mapped onto the lattice spring model (LSM), which consists of a three-dimensional network of harmonic springs. We assign a different spring constant, k, to springs localized in polymer domains and to springs located in particle regions. We then apply a stress at the boundaries of the simulation box and determine the local elastic response of the system. In this manner, we can correlate the particle distribution within the film to the mechanical properties of the material. Furthermore, by comparing the properties of the different particle-filled coatings, we can isolate the effect of the filler architecture on the mechanical behavior and the repair of the damaged substrate.

Below, we begin by describing the details of the MD and LSM simulations. We then discuss the effect of varying the particle aspect ratio on the particle−particle interactions and the localization of the particles into the notch. Next, we compare the mechanical properties of the different particle-filled systems. These findings provide guidelines for formulating nanocomposite coatings that effectively heal the surfaces through the self-assembly of the particles into the defects.

II. Numerical Method

A. Molecular Dynamics. Molecular dynamics simulations are performed using a standard "Lennard-Jones + FENE" model[7] with the LAMMPS code.[8] Nonbonded interactions between atoms i and j are of the Lennard-Jones form, shifted by the hard-core diameter r_c:

$$U_{ij}^{\mathrm{LJ}} = \begin{cases} 4\epsilon[(\sigma/(r_{ij}-r_c))^{12} - (\sigma/(r_{ij}-r_c))^{6}], & r_{ij}-r_c \le 2^{1/6}\sigma \\ 0, & r_{ij}-r_c > 2^{1/6}\sigma \end{cases} \quad (1)$$

For monomer−monomer interactions we take $\epsilon_{mm} = 1$ and $\sigma_{mm} = 1$ as units of energy and length, respectively. There is no hard core for the monomers, i.e., $r_{c,mm} = 0$. Bonds between monomers are represented by the FENE (finite extensibility nonlinear elastic) potential

$$U_{ij}^{\mathrm{FENE}} = \begin{cases} -0.5kR_0^{\,2}\ln[1-(r_{ij}/R_0)^2], & r_{ij} \le r_0 \\ \infty & r_{ij} > r_0 \end{cases} \quad (2)$$

where $R_0 = 1.5\sigma$ and $k = 30\epsilon/\sigma^2$.

Rodlike particles are modeled as a series of LJ beads "glued" together, that is, constrained to move as a rigid body. (For clarity, we reserve the term "particle" for the entire rigid-rod-like object and refer to its components as "beads". A spherical particle is, of course, a single bead.) The particle aspect ratio a is equal to the number of beads in the particle. We study the cases $a = 1$, 2, 4, 8 while keeping the particle volume constant. Thus, the bead volume must be proportional to $1/a$. If one controlled bead size by varying σ_{bb} (where bb refers to bead−bead interactions), the effect would be to make larger beads softer than smaller ones. This is undesirable in a study of excluded-volume effects. Instead, we use $\sigma_{bb} = 1$ and $\epsilon_{bb} = 1$ in all cases and vary only the hard-core diameter, $r_{c,bb}$. The diameter of a bead is $r_b = \sigma_{bb} + r_{c,bb}$, and its volume is $\pi/6(\sigma_{bb} + r_{c,bb})^3$. The volume of a particle is taken to be 8 times that of a monomer so that for $a = 1$, 2, 4, and 8 we have $r_{c,bb} = 1$, 0.587, 0.256, and 0, respectively. Parameters for the monomer−bead, mb, interaction are averages of the mm and bb parameters.

The system is bounded at the upper and lower limits, $z = \pm L/2$, by smooth surfaces and is periodic in the remaining directions. As described in ref 1, for a wall consisting of spherical particles of diameter σ located on a square lattice and spaced σ apart the potential energy of the interaction between the wall and a particle a distance r from the surface can be derived from integration over all wall particle centers, yielding

$$U^{\mathrm{LJ}} = \begin{cases} 8\pi\epsilon[{}^1/_{10}(\sigma/r)^{10} - {}^1/_4(\sigma/r)^4] & r \le 2^{1/6}\sigma \\ 0, & r > 2^{1/6}\sigma \end{cases} \quad (3)$$

The interaction between a monomer or bead and the surface is given by this potential with σ_{mm} and σ_{bb}, respectively. In this way, a monomer (bead) is at equilibrium when the distance from its center to the surface is equal to the monomer (bead) radius. The lower wall contains a notch, representing a nanoscale defect. The maximum width at the top of the notch is $6\sigma_{\mathrm{mm}}$, and the notch depth is $4\sigma_{\mathrm{mm}}$. The dimensions of the simulation box (excluding the notch) are $20\sigma_{\mathrm{mm}} \times 20\sigma_{\mathrm{mm}} \times 20\sigma_{\mathrm{mm}}$.

A time step of $\Delta t = 0.006$ is used (the monomer mass being taken as unity); times are in units of $(m_{\mathrm{mm}}\sigma_{\mathrm{mm}}{}^2/\epsilon_{\mathrm{mm}})^{1/2}$. All systems are equilibrated (at NVT) for at least 2×10^6 time steps followed by production runs of $(5-40) \times 10^6$ time steps.

Chains of length $N = 40$ are used. All simulations are performed at a reduced density $\rho = 0.85$. The reduced density of each component is $\rho_i = n_i/V\sigma_{ii}{}^3$, and the total reduced density is $\rho = \sum_i \rho_i$. The system contains 126 polymer chains and, for a particle-filled melt, 178 particles. For a bulk polymer melt at this density, we find $R_g{}^2 = 10.45$ for $N = 40$, $R_g{}^2 = 4.92$ for $N = 20$, and $R_g{}^2 = 2.22$ for $N = 10$ (where R_g is the chain radius of gyration) which agrees with earlier simulations.[7]

B. Lattice Spring Model. Once we obtain the equilibrium structure of the system, we use this information as the input into the lattice spring model (LSM).[9−13] We utilize a Born LSM[14] in order to capture the micromechanical deformation of the coated substrate in a computationally efficient manner. The LSM is a numerical technique for discretizing linear elasticity theory and consists of a network of springs connecting regularly spaced sites or nodes. The energy associated with the mth node is given by ref 14

$$E_m = \frac{1}{2}\sum_n (\mathbf{u}_m - \mathbf{u}_n)\cdot\mathbf{M}_{mn}\cdot(\mathbf{u}_m - \mathbf{u}_n) \quad (4)$$

where the summation is over all nearest- and next-nearest-neighboring nodes. Here, $\mathbf{u}_m$ is the displacement of the mth node from its original position and $\mathbf{M}_{mn}$ is a matrix containing the force constants (stiffness) for the spring between nodes m and n. The springs have two different types of force constants, central and noncentral. The central force constant energetically penalizes spring extension, while the noncentral force constant penalizes the rotation of springs from their original orientation. The Young's modulus, E, and Poisson's ratio, ν, are related to the force constants by the following equations:[14]

$$E = \frac{5k(2k + 3c)}{4k + c} \qquad \nu = -\frac{k - c}{c + 4k} \quad (5)$$

where k and c are the central and noncentral force constants, respectively. The force constants are initially associated with the nodes. Nodes are assigned different values depending upon their location in the material. In particular, $k = 100$ in the substrate and particles and $k = 1$ in the polymer matrix. This choice for the relative stiffness of the different components is consistent with experimental values for particles and polymers in filled polymeric systems.[15] The force constants assigned to the springs are then averaged from the nodes that they connect. Here, we set $c = 0$, yielding a value of $\nu = -{}^1/_4$ in both the polymer and particulate regions. This choice can be justified by noting that stress and strain concentrations in heterogeneous materials generally occur due to local variations in Young's modulus, while local variations in Poissons's ratio induce negligible perturbations to the elastic fields.

The harmonic form of the energy in eq 4 results in a force term that is linearly related to the displacements. The force acting on the mth node, due to the local displacements of its neighboring nodes, is given by

$$\mathbf{F}_m = \sum_n \mathbf{M}_{mn}\cdot(\mathbf{u}_m - \mathbf{u}_n) \quad (6)$$

If forces are applied to the boundary nodes and the spring constants specified, then the nodal displacements can be obtained through a set of sparse linear equations. These equations are solved using a conjugate gradient method to find the equilibrium configuration that corresponds to no net force at each node.[9−11,13,14,16]

To present relevant deformation fields, the stress and strain tensors are calculated from the forces and displacements. The strain tensor can be obtained through a finite difference approximation of the displacement field. A central difference approximation can be used to obtain this strain tensor:[14]

$$\delta_x u_{(i,j,k)} = \frac{-u_{(i+2,j,k)} + 8u_{(i+1,j,k)} - 8u_{(i-1,j,k)} + u_{(i-2,j,k)}}{12d} \quad (7)$$

where $u_{(i,j,k)}$ is the displacement field at coordinates i, j, k, and d is the initial distance between adjacent nodes; alternatively, forward or backward approximations are considered at system boundaries. The stress tensor is directly obtainable from the forces acting on a node (the center of a cubic unit cell)[17]

$$\sigma_{ij} = \frac{\sum_m F_m \mathbf{n}_{ij}^m}{A} \quad (8)$$

Here, $\sum_m$ represents a sum over the cubic surfaces and F_m is the force on any surface m of the cubic cell, while $\mathbf{n}_{ij}^m$ is a unit vector either normal or parallel to the surface m and A is the surface area. The scalar stress and strain values quoted here correspond to the normal stress and strain components in the tensile direction.

III. Results and Discussion

A. Potentials of Mean Force. We are ultimately interested in the localization of a high concentration of nanoparticles into surface cracks and the dependence on particle shape. As a first step, we study the interaction of a single particle in a polymer melt with a flat surface. This interaction is characterized by a potential of mean force (PMF). The PMF is a measure of the

effective differences in free energy between different states of a system. These states can be characterized by one or more relevant variables. In the present case, we are mainly interested in the energy as a function of the particle's position with respect to the surface. Thus, the PMF can be thought of as an effective interaction potential between the particle and the surface as mediated by the polymer melt. We also consider the PMF between two similar particles in the melt and between a particle and surface in the vicinity of a notch tip. Each of these interactions plays a role in the aggregation of particles in a notch.

We take as a degree of freedom the distance z between the particle center and the surface (or r, the distance between the centers of two particles). The PMF, $V(z)$, is related to the probability distribution function $p(z)$ via the reversible work theorem[18]

$$V(z) = -k_B T \ln p(z) \tag{9}$$

Then, $p(z)$ is the distribution of particle positions measured over a sufficiently long MD run (on the order of 10^7 time steps) after the system has reached equilibrium. In measuring the particle−particle PMF, the distribution $p(r)$ is normalized by $4\pi r^2$ due to the spherical degeneracy.

When the effective particle−wall interaction is particularly strong (such as for large or long particles), there is a large energy barrier for a particle at the surface to move into the bulk melt. Thus, other conformations are sampled infrequently, and it is difficult to measure the depth of the energy barrier or the form of the potential over a full range of particle−wall spacings. In this case, applying a biasing potential allows the phase space of the system to be more uniformly sampled. We use the technique of umbrella sampling,[19,20] in which the particle is subjected to a harmonic potential

$$U_{umb}(z) = k(z - z_0)^2 \tag{10}$$

The particle is thus tethered at a certain distance from the wall z_0 by a spring of stiffness k. Then, the modified form of eq 9 is

$$V(z) = -k_B T \ln p(z) - U_{umb} + K \tag{11}$$

In a typical umbrella sampling run, the system samples some range of particle positions in the neighborhood of z_0. Through eq 11, it is possible to determine the relative energies of states within this range (hence the arbitrary constant K). The width of this range depends on the stiffness k. To map out the entire PMF, one performs runs over a series of z_0. The values of z_0 are chosen such that the ranges sampled by two neighboring runs have an overlapping component. The resulting potentials are made to align in this overlap region by subtracting the constant K. We now detail our findings for the potential of mean force between the particles and a flat wall, the particles themselves, and the particles and a notched surface.

1. PMF between a Particle and Flat Wall. Figure 3 shows the PMF, as a function of the distance between a particle center and the wall, for various particle shapes. For the longest particle ($a = 8$), umbrella sampling was used to measure the depth of the potential well near the wall (Figure 4). In each case, a global minimum exists where the rod lies flat against the wall. Because the rod width varies with a, the minimum is not at the same position in each case. The shape of the potential for a sphere ($a = 1$) indicates that the attraction is due to packing effects for the monomers. The global minimum occurs where the particle is adjacent to the wall (the distance between the spherical particle center and the wall is half the sphere diameter), and there is a local minimum at a distance of one monomer diameter from the global minimum. This oscillatory potential is typical of interactions between particles in a dense, liquidlike medium. For instance, Crocker et

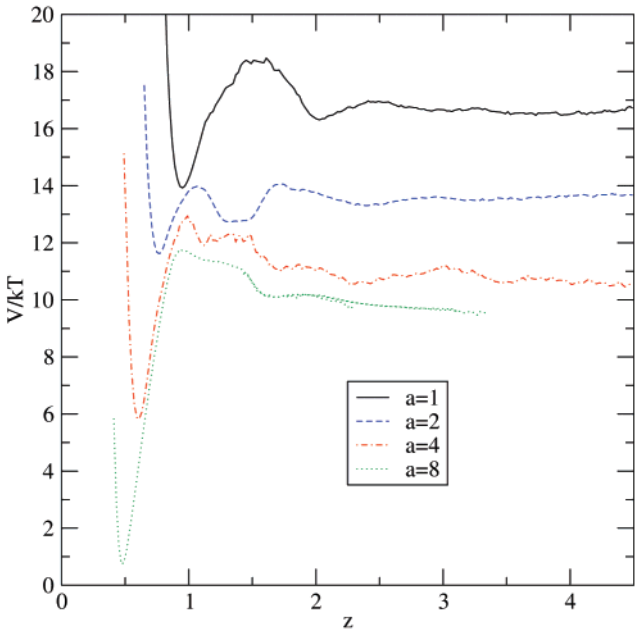

Figure 3. Potential of mean force between a particle and a flat wall located at $z = 0$ for $a = 1$, 2, 4, 8. The potential for $a = 8$ is a superposition of measurements from a series of umbrella sampling runs (shown in Figure 4). Results for other a are from a single run with no biasing potential. Potentials are shifted by an arbitrary constant for clarity.

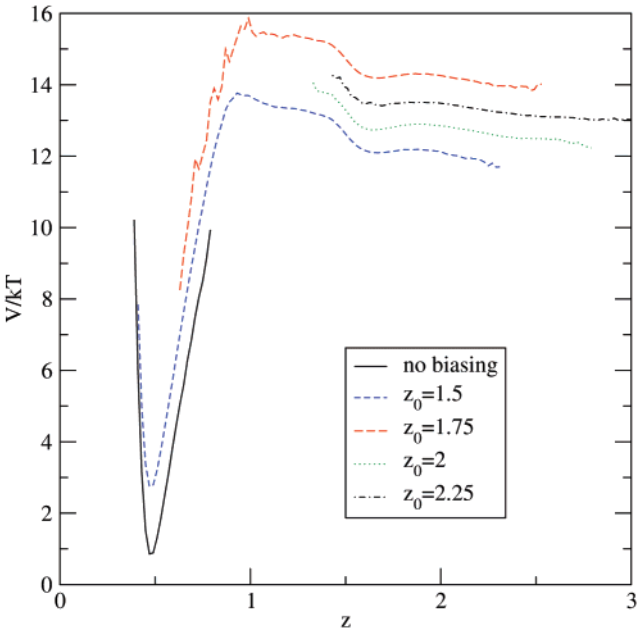

Figure 4. Potential of mean force between a particle and a flat wall located at $z = 0$ for $a = 8$ calculated from a series of umbrella sampling simulations. One run with no biasing potential is shown. All other runs used a harmonic biasing potential with a spring stiffness of $k = 20$ and were done at $z_0 = 1.5$, 1.75, 2, and 2.25.

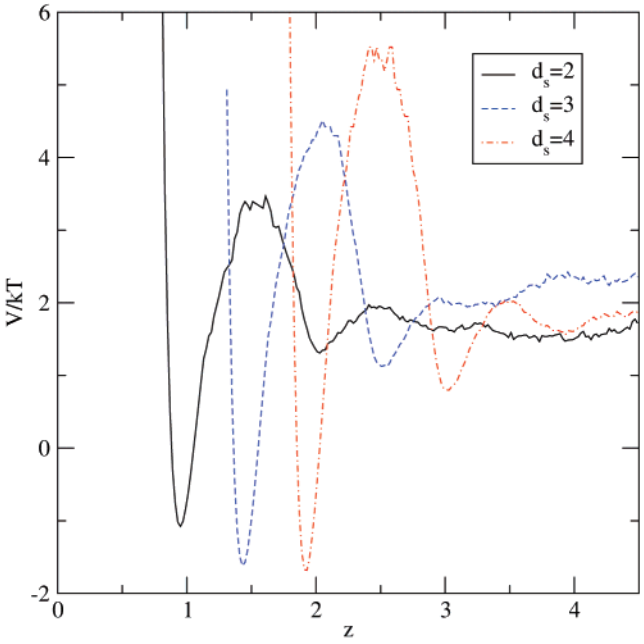

Figure 5. Potential of mean force between a spherical particle and a flat wall located at $z = 0$ for sphere diameters $d_s = 2$, 3, and 4. The sphere diameter is $d_s = \sigma_{bb} + r_{c,bb}$.

Table 1. Energy Barrier, in Units of k_BT, for a Particle to Move from a Flat Wall into the Bulk Melt (Wall → Bulk) and for a Particle To Leave the Notch Tip by Moving along One of the Side Walls (Notch → Wall), Where a Is the Particle Aspect Ratio

a	$\Delta V_{wall\rightarrow bulk}$	$\Delta V_{notch\rightarrow wall}$
1	4.47 ± 0.2	4.5 ± 0.5
2	2.36 ± 0.15	
4	7.11 ± 0.5	
8	11.02 ± 0.35	7.0 ± 0.6

Table 2. Energy Barrier, in Units of k_BT, for a Spherical Particle To Move from a Flat Wall into the Bulk Melt for Sphere Diameter d_s

d_s	ΔV
2	4.47 ± 0.2
3	6.12 ± 0.45
4	7.20 ± 0.65

al.[21] found that a monotonic attraction between two large spheres in a solution of small spheres became oscillatory when the concentration of small spheres was sufficiently high. This effect is clearly expected for the dense polymer melt considered here. It is due to the tendency of monomers to form layers at surfaces or around large particles. When the particle−wall spacing is commensurate with the width of these layers, the free energy is lowered. When it is incommensurate, the free energy is higher, and the poor packing of monomers in the interstitial region causes the particle to feel a pressure gradient driving it to one of the adjacent equilibrium states. For the spherical particles, only two energy minima are clearly observed (one for the sphere in contact with the wall and one where they are separated by one monomer layer).

The energy barrier for the particle to leave the surface (measured as the difference between the first energy minimum and the adjacent maximum) as a function of a is given in Table 1. For comparison, the energy barriers for spherical particles of different diameters were also measured (see Table 2 and Figure 5). Increasing sphere size should also enhance the depletion attraction because a larger volume is made available to the monomers when the sphere is in contact with the wall. However, the use of longer rods provides a more effective means of localizing particles at the surface than the use of larger spheres. Specifically, increasing a 8-fold, for particles of the same volume, has a larger effect on the attraction than increasing the volume of a spherical particle 8-fold. As can be seen in Table 1 and Figure 3, as a increases, the potential well near the wall becomes increasingly deep.

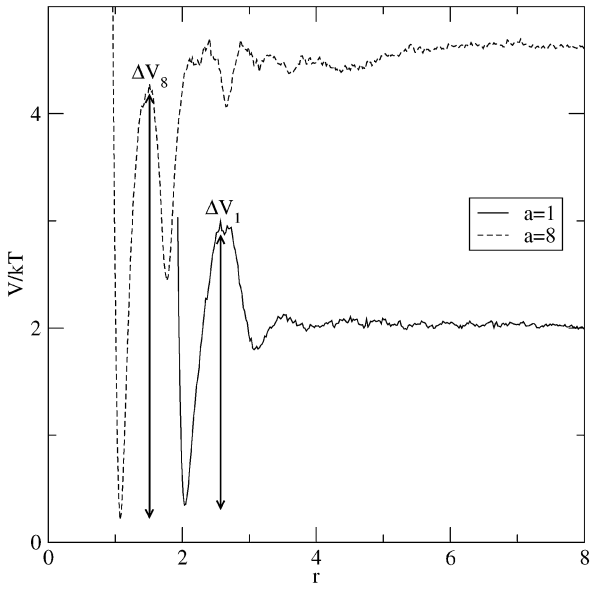

Figure 6. Potential of mean force between two like particles in a bulk polymer melt as a function of the interparticle distance r for $a = 1$ and $a = 8$. The magnitude of the respective energy barriers ΔV_1 and ΔV_8 for the separation of two particles which are in contact is shown.

2. PMF between Two Particles. We next examined the PMF between two like particles in the bulk melt in the case of spheres and of long rods (Figure 6). For large a, the rod−rod alignment could potentially affect the interaction energy. Recall that the attraction between two particles is due to the overlap of their depletion zones when they are in contact. The interaction between two spheres is characterized only by the distance between their centers. The amount of overlapping excluded volume when the spheres are in contact is less than that between a sphere and a flat surface (due to sphere curvature), leading to a lower attraction energy, but otherwise the PMF is similar.

However, when the two particles are rods, their interaction depends on their relative orientation, in addition to the center-to-center distance. Consider two rods in contact, with the minimum center-to-center distance. If the rods are parallel, their excluded volume overlap extends the full length of their axes. (Here, by "excluded volume" we are referring to the volume excluded to the monomers.) Thus, the rod−rod attraction would be stronger than the sphere−sphere attraction. In contrast, if the two rods are perpendicular, the excluded volume overlap occurs only near the point of contact, so it is much smaller than that for the parallel rods. In fact, it is also smaller than the overlap for two spheres in contact. From these considerations, we see that the attraction between two parallel rods is stronger than the attraction between two spheres and that the attraction between two perpendicular rods is weaker than the attraction between two spheres (we are refer-

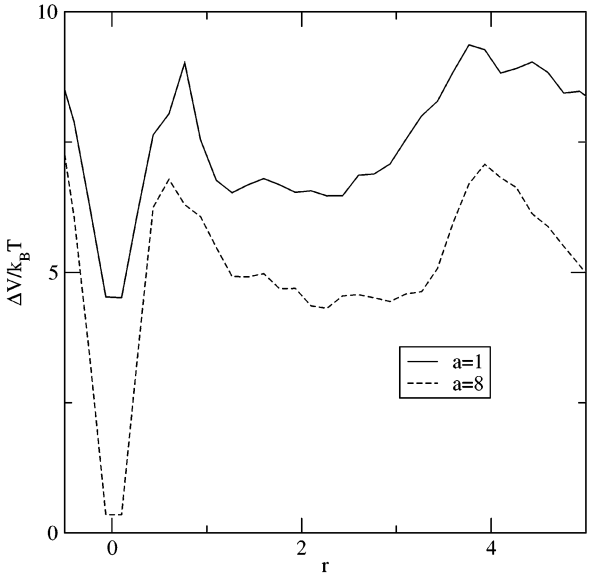

Figure 7. Potential of mean force of a particle located at the side wall of a notch as a function of the distance r from the particle center to the notch tip for $a = 1$ and $a = 8$.

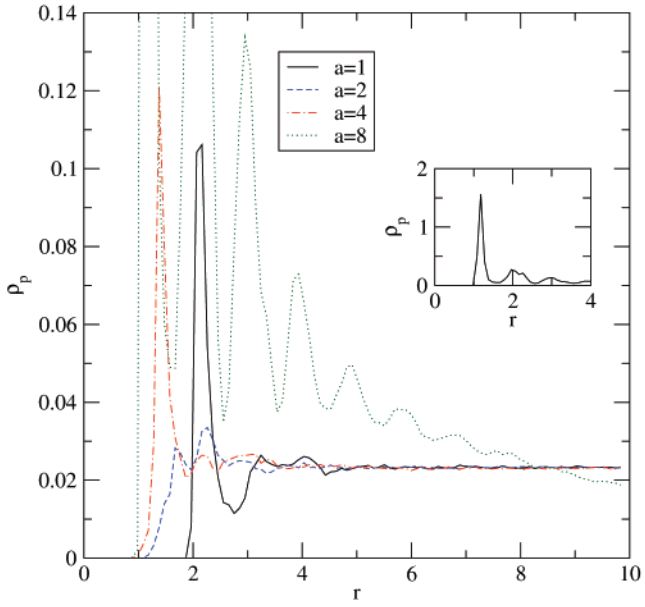

Figure 8. Radial distribution function of particle centers in a composite where $\rho_p = 0.187$ and $\rho_m = 0.663$ for various a. The inset shows the first peak for $a = 8$.

ring to rods and spheres of equal volume). From Figure 6, the ratio of rod−rod attraction to sphere−sphere attraction (as measured by the energy barriers ΔV_8 and ΔV_1) is 1.54. This indicates that rods in close proximity tend to align parallel to each other. It is well-known that in lyotropic liquid crystals[22] nearby rods tend to align their axes to increase translational entropy. In the polymer melt, it appears that the increase in volume available to the monomers serves to enhance this tendency.

3. PMF for Particle at a Notch. The key property of the polymer composites that produces their effectiveness at healing surfaces is that the filler particles are most attracted to convex surface regions (as previously seen in colloidal systems[5]), such as the notch tip, and can thus be expected to aggregate inside the notch. We calculated the PMF as a function of particle position when the particle is close to a surface notch for $a = 1$ and $a = 8$. The particle spends the majority of the time at the notch or along one of the side walls. Only rarely is the particle found in the bulk melt. Thus, we measure the potential for a particle located on a notch side wall as a function of distance from the notch tip, as shown in Figure 7.

As expected, there is an energy minimum when the particle lies at the notch tip. The energy barrier to leave the tip is listed in Table 1. The liquidlike oscillatory potential, as observed for a particle at a flat wall, is less apparent here. There is, however, an energy barrier near $r = 5$ that corresponds to the lip of the notch. As explained by Yodh et al.,[5] a particle is repelled by a concave surface region, such as the lip, for much the same reason that it is attracted to a convex surface region (that is, the change in volume available to the monomers). For both particle shapes, the energy necessary to cross the lip is small, indicating that the notch can be filled by particles diffusing across the surface, as well as those arriving directly from the bulk melt. A particle in the melt feels an attraction to a flat wall due to an overlap of the particle and the wall depletion zones that increases the free volume available to the monomers. Near a notch tip, such an overlap occurs between the particle and each side wall (as illustrated in Figure 2). Hence, the energy required to move the particle from a notch tip to a flat section of the wall should be comparable to, but less than, that needed to move a particle from a flat wall to the bulk. This is in fact what we observe (see Table 1 and Figure 7).

B. Composite Systems. We now consider the actual composite systems of interest, that is, polymer melts containing a significant loading of particles. To facilitate comparison between systems, we use roughly the same overall density as in the pure melt case, $\rho \approx 0.85$, where the monomer density is $\rho_m = 0.663$ and the particle density is $\rho_p = 0.187$. The particle volume fraction is simply $\phi_p = \rho_p\pi/6$ or $\phi = 0.0979$. The same values for the densities are used for a bulk melt, a melt near a flat wall, and a melt near a notched wall.

1. Bulk Melt Behavior. Before examining the behavior at the walls, it is necessary to understand the tendency of the particles to aggregate in the bulk. To this end, we examined the distribution of particles in a periodic system. The morphology was first characterized by measuring the radial distribution function of the particles. Results are shown in Figure 8. All of these cases show a liquidlike arrangement, with a large peak for the first layer of adjacent particles, which lie nearly in contact with the central particle. After a few oscillations, the density approaches its average value. However, the profile for $a = 2$ is noticeably different than the other cases. The first peak is much smaller and, in fact, appears to be split into two peaks of similar size. We posit that this example constitutes an intermediate case, between the symmetry of the sphere−sphere interactions for $a = 1$ and the large entropic penalty incurred by longer rods for any conformation in which nearby rods are not oriented parallel. Thus, short rods appear to be unique in that more than one particle−particle orientation are possible (due to the asymmetry) and also probable (since changes in excluded volume due to rotations are weak). As we show below, this leads to weaker ordering, and hence less dense packing, both in the bulk and near a surface. The longest rods ($a = 8$) show a greater tendency to aggregate, as indicated by a larger initial peak that is followed by a series of peaks,

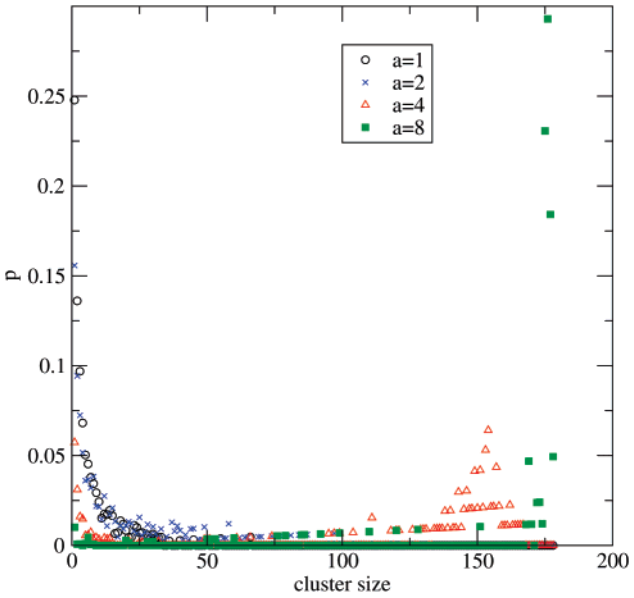

Figure 9. Particle cluster size distribution for various particle shapes in a bulk polymer melt. The distribution is weighted by the number of particles, not the number of clusters.

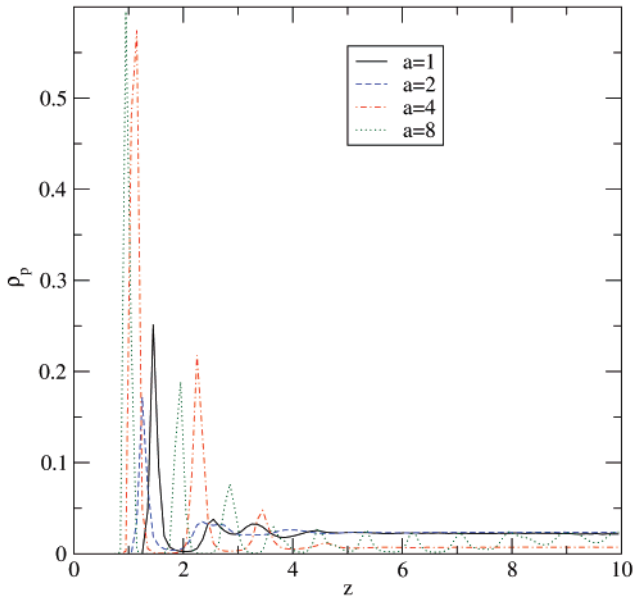

Figure 10. Particle number density in a particle-filled polymer melt with a flat wall located at $z = 0$.

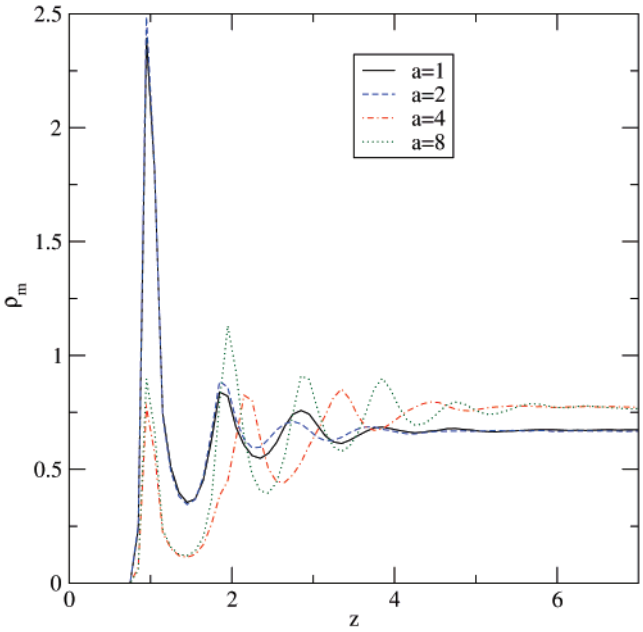

Figure 11. Monomer number density in a particle-filled polymer melt with a flat wall located at $z = 0$.

which signals long range ordering. It can also be seen that the particle density does not reach its average value at large r but continues to decrease. This indicates that the true equilibrium cluster is greater than the number of particles in our simulation. Further evidence of this is obtained by examining the distribution of cluster sizes n_c (Figure 9). Spheres tend not to aggregate significantly, and the distribution rapidly decays with increasing n_c. Short rods ($a = 2$) are little different, with only a slight increase in the amount of large clusters formed. This agrees well with the lack of ordering previously supposed. Increasing the aspect ratio to $a = 4$ shows a dramatic shift in behavior, with the majority of the particles existing in large clusters of approximately $n_c = 150$. For the longest rods, the aggregation is overwhelming, and almost no particles are observed outside of clusters. A strong peak in the distribution occurs at $n_c = 178$ (the total number of particles in the system) and even larger clusters would be expected in a bigger system.

2. Flat Walls. Having characterized particle aggregation in the bulk melt, we next consider its occurrence in the presence of a flat surface. The particle number density near a flat wall (Figure 10) is analogous to the behavior observed in the bulk. All particles tend to aggregate at the surface, with the short rods ($a = 2$) having the weakest degree of aggregation. The two longest rods examined here have multiple peaks in the density profile, a sign of long-range ordering. The increased density of particles at the surface of course implies a lower density of monomers at the surface (Figure 11).

3. Notch. We now turn to the main objective of the MD component of this work, understanding how varying a affects the aggregation and ordering of the particles inside the notch. Differences in behavior can readily be observed in the density profiles (Figure 12). For the spheres, there is a large spike in the density (representing the location of a particle center) near the notch and a smaller spike on either side wall. In contrast, the density profile of the long rods is a series of spikes, with a regular spacing, over the entire depth and width of the notch. This indicates that the rods tend to arrange into a close-packed conformation inside the notch. This high degree of ordering is most likely due to the confined geometry of the notch, which allows for fewer possible configurations. For long rods, the tendency to align reduces the situation to something resembling two-dimensional packing. Close-packed cylinders occupy a greater volume fraction of space than close-packed spheres, helping to explain why rods are better at filling the notch. Typical instantaneous conformations are shown in Figure 13 and Figure 14. The overall result is that the volume fraction of particles in the notch increases with the particle aspect ratio (Figure 15). The sole exception is for short rods ($a = 2$), which were already shown to be poor at aggregating. However, in all cases, the notch is more particle rich than the bulk.

C. Mechanical Properties. Equilibrium particle positions at a notched surface were used as input in the

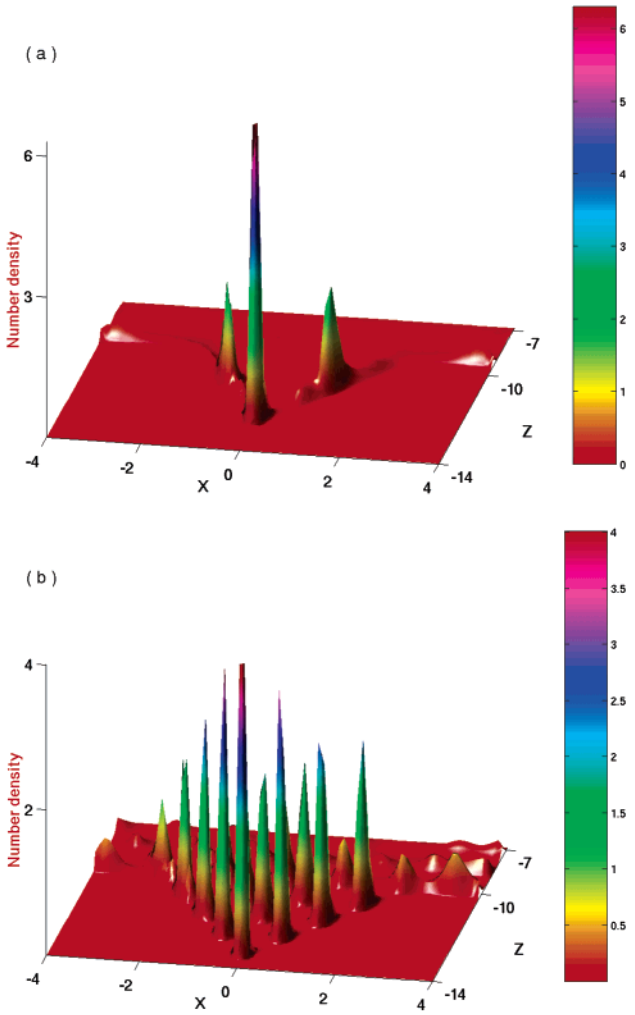

Figure 12. Two-dimensional number density profile (averaged over the invariant y direction) of particles in the notch region for (a) $a = 1$ and (b) $a = 8$.

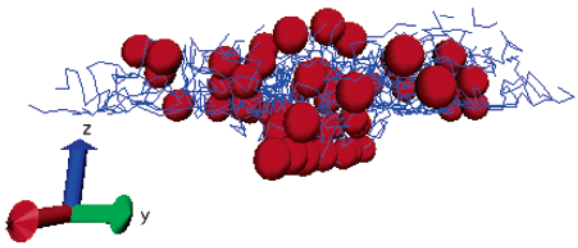

Figure 13. A representative instantaneous molecular configuration of a particle-filled polymer melt near a surface notch for spherical particles ($a = 1$). Particle beads are shown as spheres and polymer chains as lines.

LSM in order to investigate the enhanced mechanical properties of "healed" surfaces. A unit distance of σ_{mm} in the MD simulation was represented by six lattice sites on the cubic grid used in the LSM. The system considered in the LSM was the lower half of the MD simulation box (consisting of the notched wall and a portion of the bulk melt) with the "solid wall" region extended 54 lattice sites ($9\sigma_{mm}$) below the notch. Our aim was to measure the mechanical properties of a bulk solid region with a notch at its surface.

The particles were assumed to consist of a hard material similar to the substrate and springs lying in either substrate or particle regions were given a spring constant of $k = 100$. The polymer is assumed to be a

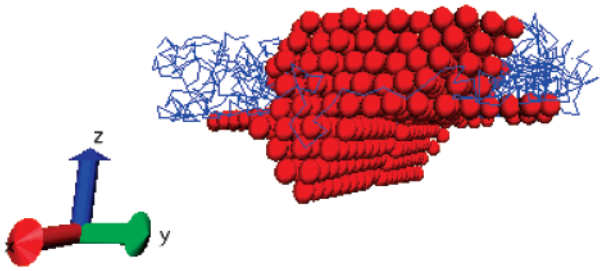

Figure 14. A representative instantaneous molecular configuration of a particle-filled polymer melt near a surface notch for rodlike particles ($a = 8$). Particle beads are shown as spheres and polymer chains as lines.

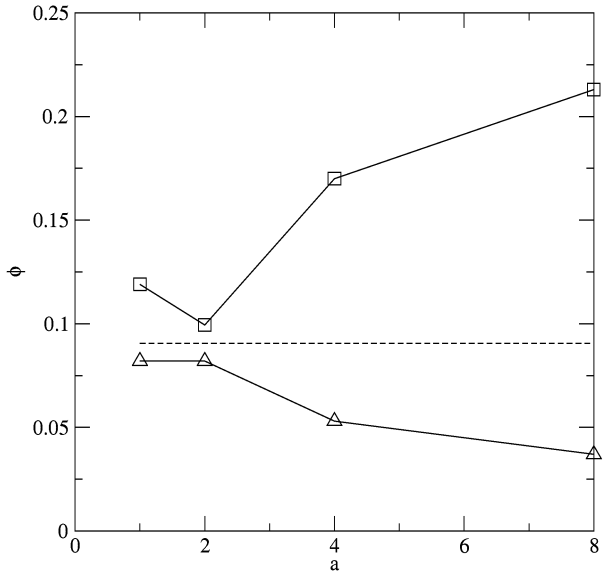

Figure 15. Average volume fraction of particles inside the notch as a function of particle aspect ratio (squares). Also shown are the average particle volume fraction of the system (dashed line) and the average volume fraction in the bulk melt in equilibrium with the notch (triangles).

soft material so that springs in the polymer-occupied regions have a spring constant of $k = 1$. We assume that there is good adhesion between the particles and monomers, as would be the case if the filler particles and polymers are chemically compatible. To focus on the role of notch filling, we consider only those particles lying within the notch and compare results for systems coated with a pure polymer layer (no particles) and with composite coatings for the various particle shapes. In this way, we can not only determine the mechanical consequences of having the particles localized in the notch but also establish the optimal particle architecture for maximizing the extent of repair.

A constant extensional force was applied in the x direction (normal to the notch axis and parallel to the surface) to the nodes on the yz boundaries of the system, and equilibrium properties were measured. The normal stress field, σ_{xx}, for a cross section of the unfilled notch is shown in Figure 16A. There is clearly a high stress concentration at the notch tip. Stress buildup can occur when the sample is subjected to an external tensile load and is responsible for the onset of crack propagation and failure of the material.

A significant reduction of the stress concentration at the notch tip is observed for the particle-filled systems. The average cross section of the stress field is shown for spheres and for the longest rods in parts B and C of

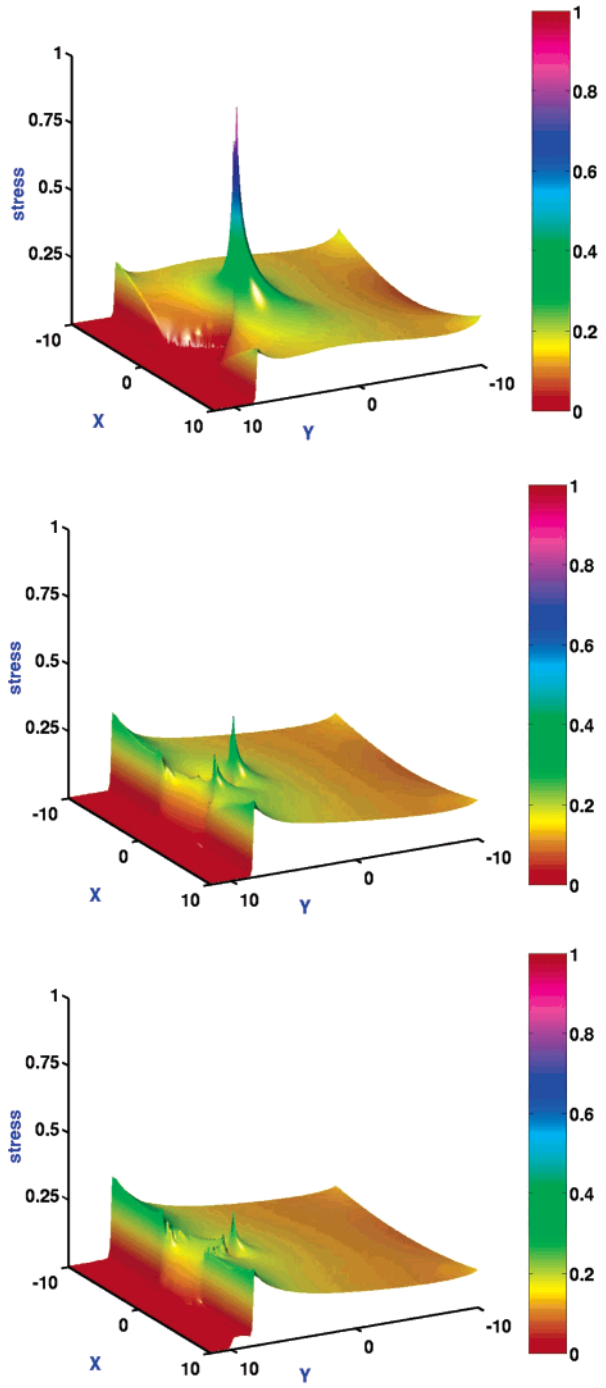

Figure 16. Two-dimensional profiles of the normal stress field (σ_{xx}) at an average cross-section for (a) no filler particles, (b) $a = 1$ particles, and (c) $a = 8$ particles.

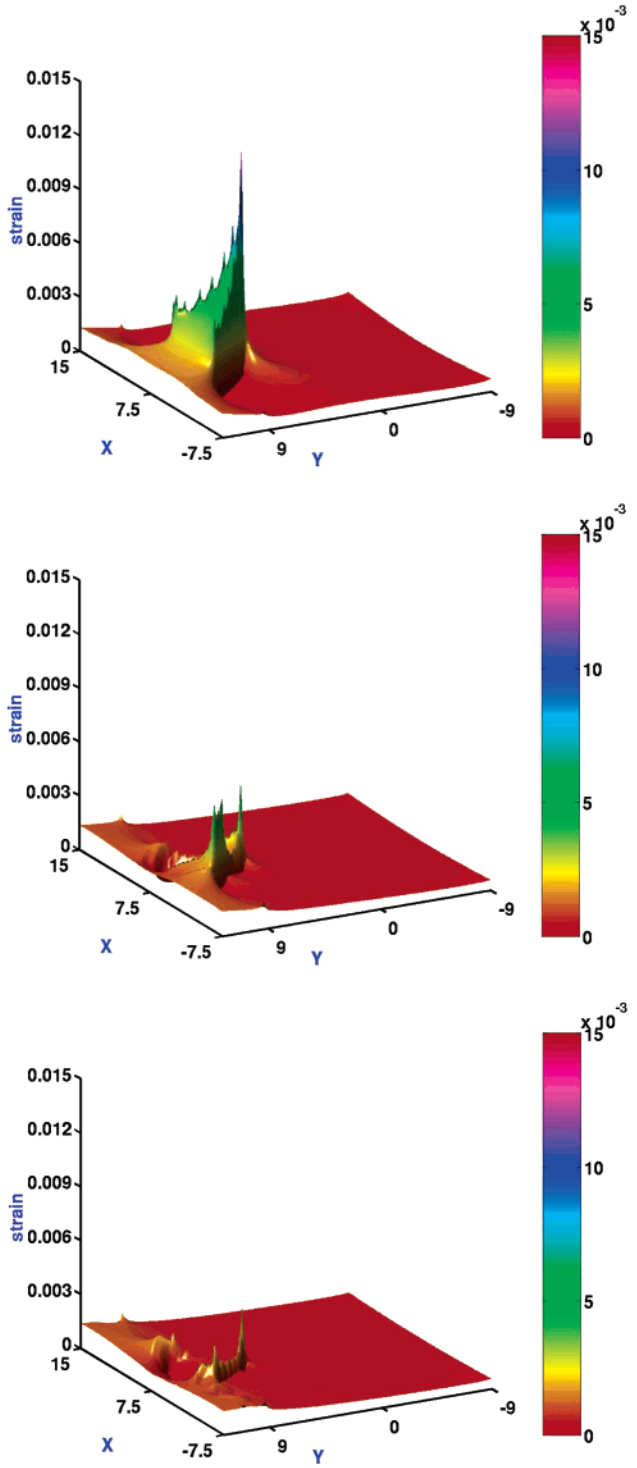

Figure 17. Two-dimensional profiles of the strain field (u_{xx}) at an average cross section for (a) no filler particles, (b) $a = 1$ particles, and (c) $a = 8$ particles.

Figure 16, respectively. The particles in the notch pack into a dense arrangement, particularly at the tip, thus forming a bridge between the two notch surfaces. This allows the stress to be transferred across a continuous region of rigid material, leading to a more even distribution. Not only is there a significant stress reduction with respect to the unfilled coating, but this reduction also increases with a. The maximum stress occurring at the notch tip has a value of 0.9462 for the unfilled melt, 0.4241 for $a = 1$ particles, and 0.317 for $a = 8$ particles.

The local normal strain u_{xx} is shown in Figure 17 for the pure polymer coating and for the composite coatings with $a = 1$ and $a = 8$ particles. Without the filler particles, the strain is highest in the soft polymer inside the notch. When spherical particles are added, the maximum strain is reduced and even further reduction occurs with the addition of long rods. For spherical particles, a noticeable peak still exists close to the notch tip. We infer that this is due to the vacancy between the particle and the notch tip. For the long rods, this peak appears much smaller. Because the rods are thinner than the spheres, they have better packing at the notch tip, further reducing the vacancy over which strain buildup can occur. Thus, not only are particles with higher a more strongly attracted to the notch but also due to their geometry they are better able to repair

the tip where crack propagation would ultimately occur. The maximum values of strain are 0.0131 for the unfilled melt, 0.0054 for $a = 1$ particles, and 0.0040 for $a = 8$ particles.

IV. Conclusion

The push to increase the sustainability of materials and reduce energy costs is driving researchers to rethink the way in which materials must be designed and fabricated. One key issue is rising to the forefront in the design of sustainable, energy-efficient systems. Specifically, there is a critical need for materials that can respond to environmental changes and perform a specific function without external intervention. This is particularly important with respect to mechanical damage, where responsive systems could prevent catastrophic failure and thus enhance the survivability and lifetime of the materials.

In this study, we attempted to address this issue by designing a coating that can actively respond to the presence of nanoscale notches, cracks, or scratches in a surface. In particular, we examined the performance of particle-filled polymer layers that were applied to a damaged surface. Our specific aim was to determine how the aspect ratio of the particles, a, affected both the localization of these solids into a notch in the substrate and the subsequent improvement in the mechanical behavior of the system. We first used MD simulations to determine how the potential of mean force between a particle and wall (and between two particles) is influenced by the value of a. This allowed us to quantify the increase in attraction between the fillers and the substrate as the aspect ratio of the particles was increased. In accordance with these findings, we observed a higher concentration of rods than spheres within the notch. We also found that longer rods tend to align in the direction of the notch and thus provide a more closely packed filling of the notch.

Having obtained the self-assembled morphology of the particle-filled coating, we then used this information as the input into the LSM, which was use to quantify the response of the quenched layer to an applied deformation. We found that systems filled with rods provide a better mechanical reinforcement than those filled with spheres of the same volume.

It is important to note that some fraction of the polymers are also localized in this damaged region. If the polymers and particles are chemically compatible, these chains provide cohesion between the fillers and the polymer coating. However, if the polymer and particles were incompatible, there would be little cohesion between these species, and the particles would decohere from the surrounding matrix, forming voids. Therefore, the chemical compatibility of the polymers in the gap also contributes to enhancing the mechanical properties of the system.

Acknowledgment. The authors gratefully acknowledge financial support from ARO and DOE.

References and Notes

(1) Tyagi, S.; Lee, J. Y.; Buxton, G. A.; Balazs, A. C. *Macromolecules* **2004**, *37*, 9160−9168.
(2) Lee, J. Y.; Buxton, G. A.; Balazs, A. C. *J. Chem. Phys.* **2004**, *121*, 5531−5540.
(3) Higgins, D. A.; VandenBout,; Kerimo, J.; Barbara, P. F. *J. Phys. Chem.* **1996**, *100*, 13794.
(4) Asakura, S.; Oosawa, F. *J. Chem. Phys.* **1954**, *22*, 1255.
(5) Yodh, A. G.; Lin, K.-H.; Crocker, J. C.; Dinsmore, A. D.; Verma, R.; Kaplan, P. D. *Philos. Trans. R. Soc. London A* **2001**, *359*, 921−937.
(6) Donev, A.; Cisse, I.; Sachs, D.; Variano, E.; Stillinger, F. H.; Connelly, R.; Torquato, S.; Chaikin, P. M. *Science* **2004**, *303*, 990−993.
(7) Kremer, K.; Grest, G. S. *J. Chem. Phys.* **1990**, *92*, 5057.
(8) Plimpton, S. J. *J. Comput. Phys.* **1995**, *117*, 1.
(9) Buxton, G. A.; Balazs, A. C. *Interface Sci.* **2003**, *11*, 175−186.
(10) Buxton, G. A.; Balazs, A. C. *Phys. Rev. E* **2003**, *67*, 031802.
(11) Shou, Z.; Buxton, G.; Balazs, A. C. *Composite Interfaces* **2003**, *10*, 343−368.
(12) Buxton, G. A.; Balazs, A. C. *Phys. Rev. B* **2004**, *69*, 054101.
(13) Buxton, G. A.; Balazs, A. C. *Mol. Simul.* **2004**, *30*, 249−257.
(14) Buxton, G. A.; Care, C. M.; Cleaver, D. J. *Model. Simul. Mater. Sci. Eng.* **2001**, *9*, 485−497.
(15) McCrum, N. G.; Buckley, C. P.; Bucknall, C. B. *Principles of Polymer Engineering*; Oxford University Press: New York, 1997.
(16) Buxton, G. A.; Balazs, A. C. *J. Chem. Phys.* **2002**, *117*, 7649−7658.
(17) Monette, L.; Anderson, M. P. *Model. Simul. Mater. Sci. Eng.* **1994**, *2*, 53−66.
(18) Chandler, D. *Introduction to Modern Statistical Mechanics*; Oxford University Press: New York, 1987.
(19) Frenkel, D.; Smit, B. *Understanding Molecular Simulation*; Academic Press: New York, 2001.
(20) Kim, E. B.; Faller, R.; Yan, Q.; Abbott, N. L.; de Pablo, J. J. *J. Chem. Phys.* **2002**, *117*, 7781−7787.
(21) Crocker, J. C.; Matteo, J. A.; Dinsmore, A. D.; Yodh, A. G. *Phys. Rev. Lett.* **1999**, *82*, 4352.
(22) Onsager, L. *Ann. N.Y. Acad. Sci.* **1949**, *51*, 627.

MA0515127